AGU PUBLICATIONS

JGR

Journal of Geophysical Research: Oceans

RESEARCH ARTICLE

10.1002/2014JC009924

Special Section:
Early scientific results from the salinity measuring satellites Aquarius/SAC-D and SMOS

The diurnal salinity cycle in the tropics

Kyla Drushka[1,2], Sarah T. Gille[1], and Janet Sprintall[1]

[1]Scripps Institution of Oceanography, University of California, San Diego, La Jolla, California, USA, [2]Now at Applied Physics Laboratory, University of Washington, Seattle, Washington, USA

Abstract Observations from 35 tropical moorings are used to characterize the diurnal cycle in salinity at 1 m depth. The amplitude of diurnal salinity anomalies is up to 0.01 psu and more typically ~0.005 psu. Diurnal variations in precipitation and vertical entrainment appear to be the dominant drivers of diurnal salinity variability, with evaporation also contributing. Areas where these processes are strong are expected to have relatively strong salinity cycles: the eastern Atlantic and Pacific equatorial regions, the southwestern Bay of Bengal, the Amazon outflow region, and the Indo-Pacific warm pool. We hypothesize that salinity anomalies resulting from precipitation and evaporation are initially trapped very near the surface and may not be observed at the 1 m instrument depths until they are mixed downward. As a result, the pattern of diurnal salinity variations is not only dependent on the strength of the forcing terms, but also on the phasing of winds and convective overturning. A comparison of mixed-layer depth computed with hourly and with daily averaged salinity reveals that diurnal salinity variability can have a significant effect on upper ocean stratification, suggesting that representing diurnal salinity variability could potentially improve air-sea interaction in climate models. Comparisons between salinity observations from moorings and from the Aquarius satellite (level 2 version 3.0 data) reveal that the typical difference between ascending-node and descending-node Aquarius salinity is an order of magnitude greater than the observed diurnal salinity anomalies at 1 m depth.

Key Points:
- Diurnal salinity throughout the tropics up to 0.01 psu
- Diurnal entrainment and precipitation drive diurnal salinity
- Aquarius ascending-descending difference exceeds day-night salinity signal

Correspondence to:
K. Drushka,
kdrushka@apl.uw.edu

Citation:
Drushka, K., S. T. Gille, and J. Sprintall (2014), The diurnal salinity cycle in the tropics, *J. Geophys. Res. Oceans*, *119*, 5874–5890, doi:10.1002/2014JC009924.

Received 1 MAR 2014
Accepted 19 AUG 2014
Accepted article online 23 AUG 2014
Published online 10 SEP 2014

1. Introduction

The diurnal cycle of salinity is important because it influences upper ocean stratification, which in turn affects sea surface temperature (SST) and air-sea fluxes of heat and momentum. Solar insolation varies throughout the day, which drives diurnal cycles in the upper ocean that include variations in temperature [*Kawai and Wada*, 2007], momentum and shear [*Cronin and Kessler*, 2009], turbulence and mixed-layer depth [*Lien et al.*, 1995]. Diurnal variability is increasingly thought to play an important role in the coupled air-sea system [*Kawai and Wada*, 2007; *Clayson and Bogdanoff*, 2013]: models driven with subdaily forcing more accurately reproduce oceanic and atmospheric variations at diurnal and intraseasonal time scales compared to those forced with daily fields [e.g., *McCreary et al.*, 2001; *Bernie et al.*, 2005; *Woolnough et al.*, 2007]. Diurnal variations of turbulence and mixing at the base of the mixed layer also appear to modulate the downward transfer of energy [*Woods et al.*, 1984; *Danabasoglu et al.*, 2006], suggesting that diurnal variability may be important for the interaction of the surface layer and the deeper ocean [*Bernie et al.*, 2005]. Model sensitivity studies have shown that a diurnally varying mixed layer is necessary in order to accurately reproduce intraseasonal (i.e., Madden-Julian Oscillation, MJO) variations. The formation of a diurnal warm layer results in a warmer daily-mean SST, which affects convection and winds; wind and convective anomalies associated with the MJO modulate the formation of diurnal warm layers [*Bernie et al.*, 2005; *Shinoda*, 2005; *Woolnough et al.*, 2007; *Li et al.*, 2013]. There are thus feedbacks between diurnal and intraseasonal air-sea processes in the tropics, illustrating the importance of understanding what drives upper ocean stratification on diurnal scales. None of the studies of diurnal-intraseasonal feedbacks considered the role played by salinity. Since salinity controls upper ocean stratification throughout much of the tropics [*Sprintall and Tomczak*, 1992; *de Boyer Montégut et al.*, 2007], it can potentially play a role in the coupled air-sea system [*Anderson et al.*, 1996]. Understanding where and why diurnal salinity variations are strong will help to model this complex system.

Although the average diurnal sea surface salinity (SSS) cycle is likely small [~0.005 psu; *Cronin and McPhaden*, 1999], there are still good reasons for investigating the drivers of diurnal salinity variability. First, salinity can indirectly affect SST by modulating upper ocean stratification [*Lukas and Lindstrom*, 1991; *de Boyer*

Montégut et al., 2007], and hence the amount by which the sea surface warms and cools during the course of a day [*Soloviev and Lukas*, 2006]. Understanding where and when diurnal salinity variations are large will allow us to assess their role in the coupled air-sea system, and will help guide decisions about whether sub-daily salinity variations should be included in models. Second, differences between the descending and ascending nodes of the Aquarius satellite, which sample in the morning and evening, respectively, can introduce a day-night bias in SSS retrievals. A knowledge of diurnal SSS variations will help unravel this bias.

Despite recent progress toward quantifying global near-surface salinity variations [e.g. *Roemmich and Gilson*, 2009; *Durack and Wijffels*, 2010], the understanding of salinity variability on shorter timescales is still limited [*Maes et al*., 2013]. Quantifying the daily salinity cycle is a challenge: in contrast to SST, which is controlled by a fundamentally diurnal process—solar insolation—SSS is governed by several processes, including precipitation, evaporation, and mixing, that are not exclusively driven by diurnal processes and are not necessarily in phase. An additional challenge is that precipitation-driven salinity anomalies often do not penetrate more than 1 m into the water column [*Henocq et al*., 2010], which is above the shallowest depth measured from most in situ platforms such as typical Argo floats, ship-board thermosalinographs, or expendable conductivity-temperature-depth probes. As a result, relatively few salinity observations that can be used to characterize the diurnal cycle exist for the top meter of the ocean. The goal of the present study is to determine where diurnal salinity variations are strong and to assess the forcing mechanisms that drive these variations. We use data from moorings throughout the tropics to estimate the average diurnal cycle of 1 m salinity and of precipitation, evaporation, vertical entrainment, and horizontal advection. Findings from this study may ultimately help to improve retrievals by the salinity satellite missions as well as guide future in situ and model sensitivity studies aimed at quantifying the role of diurnal salinity variations in the coupled ocean-atmosphere system.

2. Background

2.1. Drivers of Diurnal Salinity

Diurnal SST anomalies are largely driven by solar insolation, which peaks at roughly the same local time at each day [*Woods*, 1980; *Kawai and Wada*, 2007]. In contrast, it is not obvious that salinity should vary diurnally. While a handful of studies have documented strong changes in upper ocean salinity over the course of several days or less [e.g. *Anderson et al*., 1996; *Wijesekera and Gregg*, 1996; *Vialard et al*., 2009], few have evaluated whether those daily changes occur systematically, and, if so, what the implications might be in terms of potential feedbacks to the atmosphere. Changes in the salinity averaged over the mixed layer ($\bar{S}$) can be described by:

$$\frac{\partial \bar{S}}{\partial t} = \underbrace{\frac{E-P}{h}\bar{S}}_{a} - \underbrace{\mathbf{u}\cdot\nabla\bar{S}}_{b} - \underbrace{w_E\frac{\Delta S}{h}}_{c} + \epsilon, \tag{1}$$

where E and P represent rates of evaporation and precipitation, respectively; h is the mixed-layer depth (MLD); $\mathbf{u}$ is the two-dimensional horizontal velocity; w_E is the vertical entrainment velocity at the base of the mixed layer; and ΔS represents the change in salinity across the base of the mixed layer. The terms on the right-hand side of equation (1) hence represent (a) surface forcing, (b) horizontal salt advection, and (c) vertical entrainment of salt at the base of the mixed layer. ϵ represents horizontal and vertical diffusion and vertical advection. The relative amplitudes and phasing of these processes, as well as the background ocean stratification, all affect how surface salinity varies throughout the course of the day.

Diurnal precipitation is generally strongest in regions with strong mean rainfall, including the Intertropical Convergence Zone in the Pacific and Atlantic Oceans, the eastern Indian Ocean north of the equator, the western Pacific Ocean, and near the coastlines in the western side of each ocean basin [*Kikuchi and Wang*, 2008]. Rainfall in the tropics and subtropics typically peaks in the early morning to midmorning, with afternoon rain also common [*Janowiak et al*., 1994; *Nesbitt and Zipser*, 2003]. Tropical rainfall tends to be intermittent in space and time, leading to low-salinity surface patches [*Soloviev and Lukas*, 2006] that are mixed away within hours to days, primarily due to nighttime convective overturning in the mixed layer [*Brainerd and Gregg*, 1997; *Wijesekera et al*., 1999]. Strong rain can produce a thin, buoyant halocline that suppresses turbulent exchange with the water below, trapping atmospheric fluxes to the near surface [*Wijesekera et al*.,

1999]. The strong surface stratification produced by heavy rainfall also reduces the vertical entrainment of salt and heat [*Anderson et al*., 1996].

Wind drives evaporation, which increases SSS [*Soloviev and Lukas*, 1997, 2006], and also acts to break down surface stratification and deepen the mixed layer. Wind tends to be strongest in the morning and evening near coastlines due to land-sea heat contrasts; the amplitude of the diurnal wind signal decays with distance from shore, and the phasing is highly variable away from the coast [*Gille et al*., 2005]. In the trade wind bands of the Pacific and Atlantic Oceans, diurnal wind variations are moderately strong, though the phasing varies over small spatial scales (a few degrees of longitude and latitude) [*Gille et al*., 2005]. Evaporation is also affected by air and sea surface temperature and humidity [*Fairall et al*., 1996], which can vary diurnally. In addition to wind stress, convection that results from nighttime cooling at the sea surface causes the mixed layer to deepen, entraining deeper water into the mixed layer. Entrainment can increase or decrease surface salinity depending on the sign of the vertical salinity gradient (ΔS in equation (1)); salinity increases with depth in most regions [e.g. *de Boyer Montégut et al*., 2007], so entrainment generally causes the mixed layer to become more salty.

Diurnal warming can produce a stable daytime surface layer that traps momentum flux, enhancing surface currents [e.g., *Bernie et al*., 2007; *Cronin and Kessler*, 2009]; in the presence of a horizontal salinity gradient $\nabla\bar{S}$, this could produce diurnal salinity advection. We assume that this is the primary driver of any horizontal salt advection, i.e., the horizontal salinity gradient does not vary systematically on diurnal time scales. Although diurnal variations in diffusive processes have been observed [e.g., *Lien et al*., 1995], we assume that their impacts on near-surface salinity are negligible.

For equation (1) to hold true, salinity anomalies resulting from each of the processes on the right-hand side must be incorporated into the mixed layer on time scales at least as fast as the equation is evaluated: in this case, hours. However, it actually takes hours or longer for precipitation anomalies to be distributed throughout the mixed layer: rain forms thin, stable surface lenses that disperse within a few hours due to mixing, diffusion, and/or advection [*Brainerd and Gregg*, 1997; *Wijesekera et al*., 1999; *Tomczak*, 1995]. For a given rain event, the depth of the resulting fresh lens depends on the strength and duration of the rainfall and the local wind speed [*Miller*, 1976] as well as the size of the rain drops [*Katsaros and Buettner*, 1969]. Early laboratory experiments showed rain penetrating to $<$10 cm; observational studies have revealed rain-formed lenses ranging in thickness from tens of centimeters [*McCulloch et al*., 2012; *Reverdin et al*., 2012] to meters [*Price*, 1979; *Soloviev and Lukas*, 2006] to over 10 m [*Wijesekera et al*., 1999]. The depth to which evaporation modulates near-surface salinity is not well understood because it is so difficult to measure [*Yu*, 2010], and few studies have presented observations of near-surface salinity anomalies resulting from evaporation. For example, *Soloviev and Vershinsky* [1982] observed a $\sim$0.02 psu salinity increase in the top 0.5 m that may have been caused by evaporation, but the uncertainty on the measurement was as large as the signal. More recently, *Asher et al*. [2014a], using a towed surface salinity profiler, found salt-enhanced surface lenses around 0.5 m thick in the subtropical North Atlantic. They noted that moderate winds are needed to evaporate enough water to produce a measureable surface salinity anomaly, but winds stronger than a few m s^{-1} destroy the ability of the surface to support salty anomalies.

A modified version of equation (1) is thus needed to explain salinity anomalies at a discrete depth on time scales faster than 1 day. For an instrument at a depth of 1 m, the salinity change dS_1 measured during a short time step dt (e.g., dt=1 h) can be approximated by the following:

$$dS_1 \approx \int \frac{E}{h_E} S_1 dt - \int \frac{P}{h_P} S_1 dt - \int \mathbf{u}_1 \cdot \nabla S_1 dt - \frac{dh\Delta S}{h}. \quad (2)$$

Equation (2) takes into account the depth to which salinity anomalies resulting from precipitation and evaporation penetrate prior to being mixed or advected away, denoted h_P and h_E, respectively. When h_E or h_P are thinner than 1 m (and hence the associated salinity anomaly is not detected at 1 m depth), the evaporation or precipitation term is set to zero. Vertical entrainment is assumed to result from the mixed layer deepening by an amount dh, so vertical velocity is approximated as dh/dt; the associated salinity anomaly is assumed to be distributed throughout the mixed layer and hence is scaled by MLD (h). Horizontal advection is assumed to result from the near-surface current $\mathbf{u}_1$ acting on the background horizontal salinity gradient ∇S_1.

Results from previous studies examining diurnal salinity cycles have suggested that vertical entrainment may be the dominant driver of diurnal SSS: *Cronin and McPhaden* [1999] used 1 m data from several TOGA-COARE

moorings in the western Pacific Ocean to show a $\pm$0.005 psu daily salinity cycle with a maximum in the early morning, despite strong local rainfall at that time. They suggested that nighttime surface cooling drives overturning in the mixed layer and entrains deeper, saltier water, producing the early morning salinity maximum. *Cronin and McPhaden* [1999] also showed that the diurnal salinity signal at 3 m depth was substantially weaker than that at 1 m depth. *Reverdin et al.* [2012] showed the average daily salinity cycle in two tropical regions based on data from surface drifters at 15–50 cm depth. In the southwest tropical Pacific Ocean, they found an early morning salinity minimum (i.e., a signal with opposite phasing to that observed by *Cronin and McPhaden* [1999]) and suggested that strong nighttime rainfall increases surface stability and hence reduces vertical entrainment. Though the studies of *Cronin and McPhaden* [1999] and *Reverdin et al.* [2012] found systematic diurnal salinity cycles, in both cases, the statistical uncertainties on the estimates were nearly as large as the signals themselves. Recently, J. E. Anderson and S. C. Riser (Near-surface variability of temperature and salinity in the near-tropical ocean: Observations from profiling floats, submitted to *Journal of Geophysics Research*, 2014) used specialized Argo floats that profile to within $\sim$0.2 m of the sea surface to quantify the diurnal cycle of near-surface salinity in several regions. They showed a diurnal salinity anomaly on the order of 0.1 psu at 0.2 m depth, which is smaller by an order of magnitude at 1 m depth, roughly consistent with the result of *Cronin and McPhaden* [1999]. To our knowledge, these are the only studies that have considered systematic diurnal salinity anomalies. Their findings highlight the following hypotheses: (a) the phasing and amplitude of diurnal SSS vary spatially; (b) vertical entrainment at the base of the mixed layer is an important driver of diurnal SSS variations; (c) day-to-day variability in subdaily salinity may smooth the average diurnal signal; and (d) diurnal salinity variations decrease substantially with depth, even within the top tens of centimeters of the water column. In the present study, we use salinity data at 1 m depth from moorings to assess these hypotheses.

3. Data and Methods

3.1. Moorings

We used data from moorings in the Tropical Atmosphere Ocean (TAO) mooring array, which are distributed by the TAO Project Office of the Pacific Marine Environmental Laboratory (PMEL) at the National Oceanic and Atmospheric Administration (NOAA). Only the data with the highest level of accuracy (quality control flags 1 or 2) were used. At 47 mooring sites, at least 1 year of hourly salinity data ($>$8760 data points) were available; an additional 24 moorings had hourly salinity with $<$1 year of high-quality data. Where available, we also utilized other hourly measurements made at the moorings: precipitation and winds (typically measured 4 m and 3.5 m above the sea surface, respectively); near-surface horizontal currents at 10 m depth; and salinity and temperature at all available depths throughout the water column. Three moorings had hourly measurements of both temperature and salinity data with $\leq$10 m vertical spacing in the top 50 m; for those sites, MLD was computed using a density-threshold criterion: density was interpolated vertically to a 1 m grid and then MLD was defined as the depth at which density decreased by 0.125 kg m^{-3} relative to 1 m density. Nine of the TAO sites also had $>$1 year of hourly evaporation estimates, which were derived using the Coupled Ocean Atmosphere Response Experiment (COARE) 3.0b bulk flux algorithm [*Fairall et al.*, 2003; *Cronin et al.*, 2006]. Note that no single site had hourly precipitation, evaporation, and MLD data.

To extract the average diurnal signal, the data were processed in a manner similar to that described by *Cronin and McPhaden* [1999]. First, a low-pass Hamming filter with a 3 day cutoff was applied to the time series at each mooring; this signal was removed, and the remaining high-frequency component was then smoothed with a 1-2-1 triangle filter. The resulting anomalies were then binned according to the local hour of the measurement. For each hourly time bin, this gave an average salinity anomaly and its uncertainty, which was calculated as the standard error, i.e., the standard deviation divided by the square root of the number of data points. Then, diurnal and semidiurnal harmonics were fit simultaneously using a weighted linear least-squares technique, where the uncertainty of the averages in each time bin provided the weighting. The minimum and maximum daily salinity anomalies were extracted from the fit, and amplitude was computed as half the difference between the maximum and the minimum. The uncertainty of the fit was used to test the significance of the diurnal signals.

The length of the salinity time series varies between individual sites. Generally, diurnal averages made with longer time series have smaller amplitudes, likely as a result of unresolved low-frequency variations that smooth out the signal when many data points are binned. To avoid biases resulting from differences in record length, we used exactly 1 year of data from each site and rejected any sites that displayed interannual variability in the diurnal

salinity amplitude. This was done by breaking the full time series into distinct 1 year segments of data and computing the diurnal phase and amplitude for each segment. Sites for which the amplitude of the different segments varied by more than 50% of the signal, or the diurnal phase for the different segments differed by more than 2 h, were excluded from the analysis: 12 sites from throughout the set of moorings were removed this way, leaving a total of 35 mooring sites for which we were confident that the diurnal salinity anomalies could be computed.

3.2. Aquarius Data

The Aquarius satellite is in a polar sun-synchronous orbit and so sees the Earth at the same two times each day, crossing the equator at roughly 06:00 local time (descending nodes) and 18:00 (ascending nodes) [*Lagerloef et al*., 2008]. As a result, any uncorrectable noise that varies with the time of day or the direction of the satellite will produce biases between the ascending and descending nodes of the orbit. For example, radio-frequency interference that is sampled at different look angles during ascending and descending nodes introduces a bias in some regions (G. Lagerloef, personal communication, 2014), which may mask ascending-descending differences in surface salinity that arise from the actual diurnal salinity cycle. In section 5.2, we estimate the ascending-descending differences in Aquarius salinities. We use the Aquarius Level 2 Combined Active-Passive (CAP) V3.0 data set, which has the most up-to-date (as of August 2014) ascending/descending bias corrections. This product was obtained from the NASA Physical Oceanography Distributed Active Archive Center (PO.DAAC). The CAP algorithm corrects Aquarius radiometer measurements using simultaneous observations from the onboard scatterometer [*Yueh*, 2013]. The data set consists of along-track salinity and wind observations for each of the three radiometers [*Le Vine et al*., 2007]. The satellite samples each 1.44 s, giving ~9.5 km along-track measurement spacing; each orbit repeats every 7 days. Two years of Aquarius data, from January 2012 to December 2013, were used in this study.

3.3. Ancillary Data

We used several additional data sets to evaluate the salinity observations in the context of atmospheric forcing and background ocean conditions. The Monthly Isopycnal and Mixed-layer Ocean Climatology (MIMOC) [*Schmidtko et al*., 2013] database provided information about the mean ocean stratification. This product is based primarily on Argo profiling float data, and includes temperature and salinity at standard depth levels (5 m vertical resolution in the top 100 m), as well as MLD, on a monthly, 0.5° horizontal grid. Climatological zonal and meridional gradients of surface salinity were estimated using a central difference method.

Global observations of evaporation came from the Hamburg Ocean Atmosphere Parameters and Fluxes from Satellite Data Set version 3.2 [HOAPSv3.2; *Fennig et al*., 2012] which is derived from Special Sensor Microwave Imager (SSM/I) satellite data and is available as a 6 h composite on a 0.5° grid. Precipitation came from the Tropical Rainfall Measuring Mission (TRMM) 3B42 version seven data set, which is produced from satellite-based radar, microwave, and visible infrared observations and is available on a 3 hourly, 0.25° horizontal grid [*Huffman et al*., 2007]. The evaporation and precipitation data sets were smoothed to a 1° spatial grid and the timestamp for the data in each grid box was converted to local time based on its longitude. The diurnal cycle at each grid point was extracted using a methodology similar to that used for the mooring data: the time series were filtered to isolate high-frequency variations, then the 24 h harmonic was fit to the filtered data (as these were 6 and 3 hourly fields, the semidiurnal harmonic was not included in the fit). This gave maps of the diurnal amplitude of evaporation and precipitation. Using 6 or 3 hourly data to compute the diurnal cycle likely underestimates the signal; we thus use these diurnal amplitude maps as a way to assess where diurnal evaporation and precipitation are likely to be relatively strong rather than to produce high-accuracy estimates of the diurnal variation of these processes. Finally, shortwave radiation, net heat flux, and wind stress from the TropFlux product were used to compute mean Monin-Obukhov length scales [e.g., *Venkatram*, 1980], which can be used to relate atmospheric conditions to properties of the mixed layer. TropFlux is computed using the COARE v3 bulk flux algorithm applied to a combination of ERA-I reanalysis ISCCP surface radiation, and is available on a daily, 1° grid throughout the tropics [*Kumar et al*., 2012].

4. Observations

4.1. Variations in the Western Pacific Warm Pool

Figure 1 shows 20 days of data from the mooring at 156E,2N in the western Pacific Ocean, which is typical of many of the mooring sites. Temperature at 1 m depth has a strong diurnal signal, peaking in the late

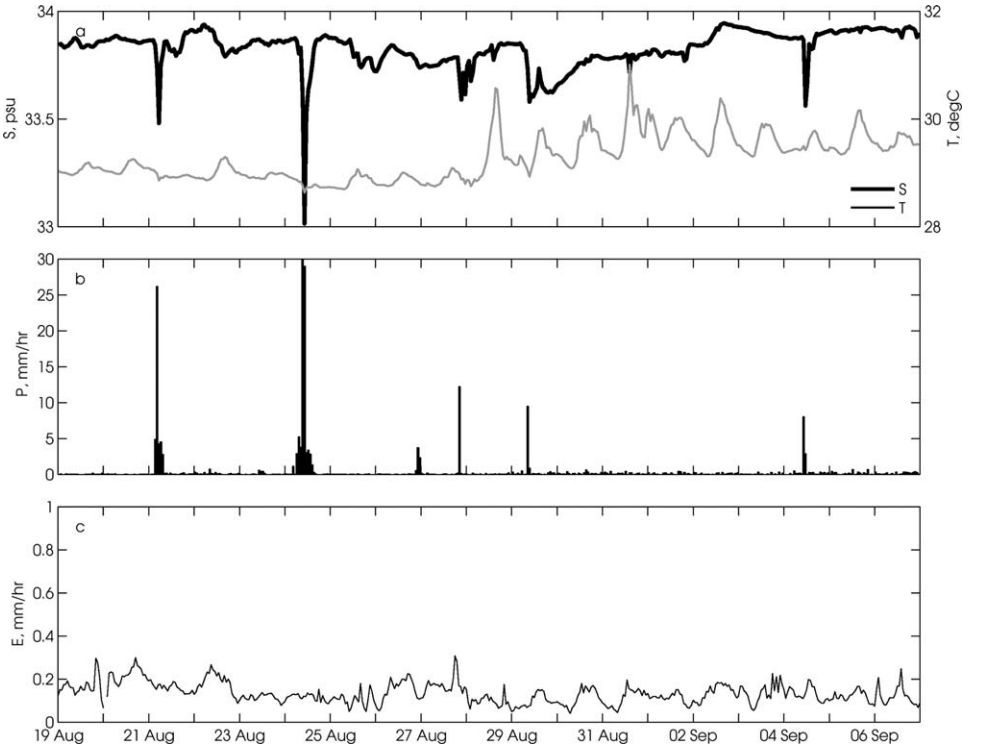

Figure 1. Mooring observations in the western Pacific warm pool during 2006. (a) 1 m salinity (thick) and temperature (thin); (b) precipitation; (c) evaporation. All measurements were made at the 156E,2N mooring site, except evaporation, which was made at the 165E,0N mooring. Ticks along the *x* axis correspond to midnight, local time.

afternoon each day with an anomaly of 0.2–0.5°C (Figure 1a). In contrast, 1 m salinity does not follow any obvious daily cycle, and instead displays high-frequency variations superimposed on slower (days or longer) variability. Rainfall is generally near zero except for occasional events with rain rates exceeding 10 mm hr^{-1} that typically persist for a few hours and drive fresh salinity spikes of 0.2–0.8 psu (Figure 1a). Evaporation (taken from the nearby mooring at 165E,0N, as there are no hourly evaporation data at 156E,2N) varies erratically (Figure 1c). Evaporation rates are typically around 0.15 $\pm$ 0.05 mm hr^{-1}, which is 10 to 100 times weaker than the rain events, suggesting that at this location evaporation has much less influence than rainfall on salinity variations faster than a day. There are also strong salinity anomalies that do not appear linked to either rainfall or evaporation (e.g., the 0.1 psu freshening on 25 August). These are likely produced by horizontal advection (for example, advection of a fresh lens produced by recent, nearby rainfall) [*Wijesekera et al*., 1999], though surface currents at this site are not available for this time period so this cannot be verified.

During the strong squall on 24 August, a total of around 74 mm of precipitation fell over several hours, driving a freshening of 0.84 psu (Figure 1a). From equation (2), this suggests that the thickness of the rain-formed surface lens (h_P) was around 3 m. Repeating this computation for the other rain events seen in Figure 1b gives similar estimates for h_P. It is more difficult to estimate the effect of evaporation on 1 m salinity because little is known about the impacts of evaporation-driven SSS anomalies on the near-surface salinity structure [e.g. *Yu*, 2010]. We estimate h_E very roughly as the depth to which a theoretical water parcel at the surface sinks after undergoing a small salinity increase. Based on evaporation rates ranging from 0.1 to 0.4 mm hr^{-1} and a density profile from the MIMOC climatology (interpolated linearly to the sea surface), and neglecting the effects of evaporation on SST (and hence on near-surface stability), we estimate that h_E is around 1 m to 2 m, consistent with an estimate of 0.5 m made by *Asher et al*. [2014a] from observations in the North Atlantic. This suggests that an evaporation-driven salinity anomaly could be detected in 1 m salinity data. From equation (2), an evaporation rate of 0.15 mm hr^{-1} applied to the surface of a layer having thickness h_E=1 m would increase salinity at a rate of 0.005 psu hr^{-1}, which would be overwhelmed by the precipitation-driven anomalies during squalls. In other words, strong rain events dominate local salinity on timescales less than a day. However, because evaporation is always nonzero, it contributes significantly

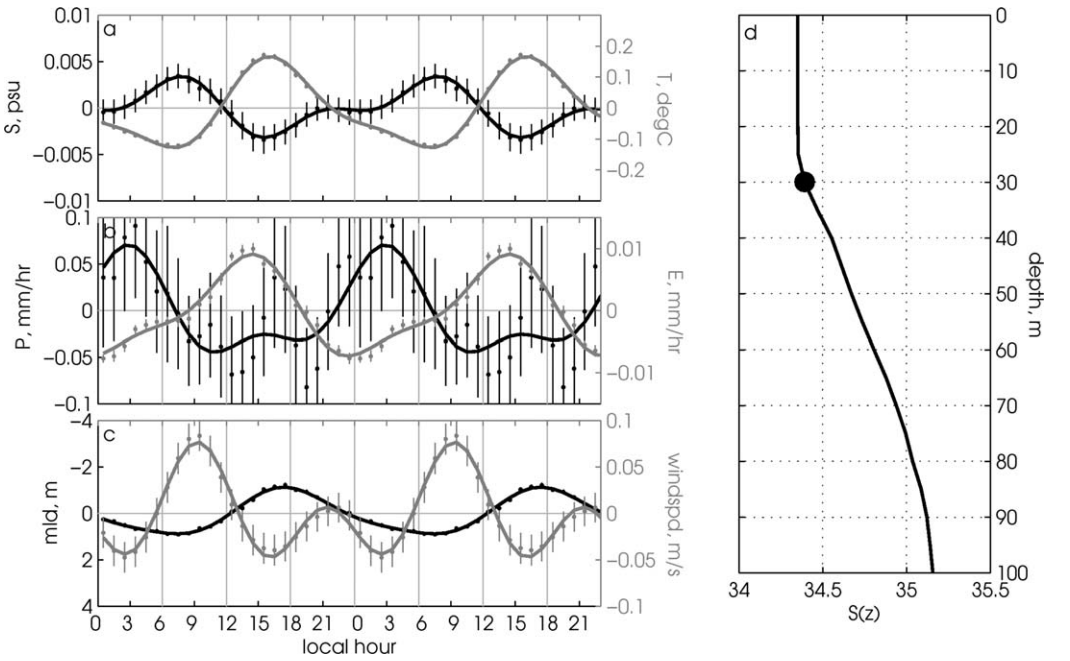

Figure 2. Daily cycles from mooring observations in the western Pacific warm pool: (a) 1 m salinity (black) and temperature (gray); (b) precipitation (black) and evaporation (gray); (c) MLD (black; note the inverted *y* axis, i.e., positive values indicate deeper mixed layers) and wind speed (gray). The markers and vertical lines represent the average and standard error of all daily anomalies within a given hourly time bin, where daily anomalies were computed by filtering hourly data with a 3 day high-pass filter and then smoothed with a 1-2-1 triangle filter. The solid lines represent the diurnal plus semidiurnal fits to the binned data, and the dotted lines represent the uncertainty on these fits (negligible for the SST signal). All data are plotted as anomalies with respect to the mean, so positive values of a given variable indicate more of that variable at a given hour of day, and negative values indicate less of that variable. Two diurnal cycles (48 h) are shown. (d) Climatological salinity profile (line) and MLD (circle) at the mooring site, from the MIMOC data set. As in Figure 1, all measurements were made at the 156E,2N mooring site, except evaporation, which was made at the 165E,0N mooring, and MLD, which was made at the 154E,0N site.

to the long-term salinity balance: for example, integrated over the 20 day record shown in Figure 1, the evaporation and precipitation nearly cancel each other out.

Figure 1 suggests that if rain events occurred at the same time each day, they would drive a strong (order 0.1 psu) diurnal salinity cycle. However, precipitation is clearly irregular and episodic: some days see zero rainfall and other days experience one or more brief episodes that do not necessarily occur at the same time (Figure 1b). To assess whether there are systematic diurnal salinity variations, we bin the anomalies of each variable by hour of day, as described in section 3.

Salinity exhibits a clear diurnal cycle at 156E,2N, though its amplitude is small (0.005 psu; Figure 2a). Salinity is minimum at 15:00 (local time), increases rapidly until 21:00, then weakens slightly for several hours before increasing from 01:00 until its peak at 07:00, after which it freshens quickly from 08:00 to 14:00. The daily salinity mirrors that of temperature, which peaks at 15:00 and is minimum at 07:00; the rate of cooling during the night also slows between 22:00 and 03:00 (Figure 2a). Note that the uncertainty estimates on the temperature anomalies are too small to see, which indicates that the strength and amplitude of the temperature signal vary little from day to day, as can be seen in Figure 1a.

The binned precipitation data reveal a noisy but statistically significant diurnal cycle, with a maximum in the morning between 00:00 and 06:00 (Figure 2b). Average precipitation anomalies are $\sim$0.07 mm day^{-1}, three orders of magnitude smaller than precipitation rates during individual squalls (Figure 1b). This is because rain rates are generally low: only 25% of the precipitation observations at this mooring site are nonzero, and only 5% exceed 5 mm hr^{-1}. When only observations with nonzero rainfall were averaged, the diurnal signal had an amplitude around $\sim$3 times larger than seen in Figure 2b, but the phasing was the same and the distribution of data points in each time bin was roughly equal. This illustrates that although precipitation peaks in the morning, rain falls at all times of day. As a result, the binned averages are noisy. The total precipitation anomaly from 00:00 to 08:00 is around 0.4 mm. Integrated over a 3 m thick layer having a salinity of 34.4 psu (Figure 2d), this would produce a total salinity anomaly of around -0.004 psu. This

is the correct order of magnitude to produce the freshening observed from 07:00 to 15:00 (Figure 2a); however, the freshening occurs several hours later than the rainfall. We hypothesize that the rain-formed lenses are initially <1 m thick and hence are not detected at the moorings; instead, the freshening at 1 m depth begins a few hours after the strongest rainfall, when positive wind anomalies (Figure 2c) mix the surface lenses downward.

The bin-averaged anomalies reveal a significant daily cycle in evaporation, with a peak at around 14:00 (Figure 2b). Both evaporation and 1 m temperature have similar phasing, with a late afternoon peak and a morning minimum. This is the case at nearly all sites (not shown); in contrast, diurnal wind stress peaks throughout the day depending on the location, suggesting that temperature changes drive the diurnal signal in evaporation. The composite evaporation is around 0.01 mm hr^{-1}, which is around 10% of the mean evaporation signal (Figure 1c). The total evaporation anomaly between 09:00 and 19:00 is around 0.06 mm; averaged over a layer h_E=1 m thick, this would produce a salinity anomaly of around 0.002 psu. As was seen for precipitation, there is a lag of several hours between the positive evaporation anomalies and the increase in salinity at 1 m depth, indicating that the salinity-enhanced layer produced by evaporation may be initially trapped above 1 m.

The mixed layer starts deepening at around 15:00 and is thickest at around 06:00, before shoaling rapidly from 07:00 to 15:00 (Figure 2c). This phasing suggests that nighttime convection is responsible for the daily deepening of the mixed layer, and surface heating in the daytime causes MLD to shoal quickly. Using the observed total MLD change (dh=2 m; Figure 2c) and the climatological MLD (h=30 m) and vertical gradient of salinity at the base of the mixed layer ($\Delta S = 0.02$ psu m^{-1}; Figure 2d), equation (2) gives a nighttime entrainment salinity anomaly of +0.002 psu. Combined with the 0.002 psu salinity anomaly estimated to result from evaporation, this would balance the 0.004 psu freshening estimated to result from precipitation. However, it underestimates the 0.007 psu (peak-to-peak) salinity anomaly that is observed (Figure 2a), suggesting that smaller values for h_P and h_E might be more realistic or that other processes could be important. The zonal surface current at a nearby site along the equator (156E,0N) has a diurnal amplitude of around 0.01 m s^{-1} (not shown); applied for half a cycle to the local climatological zonal salinity gradient of around −0.01 psu deg^{-1}, this would produce a zonal salinity anomaly of around -1×10^{-5} psu, several orders of magnitude smaller than any other term. The meridional salinity advection is similarly weak: although the meridional salinity gradient is of order 0.1 psu deg^{-1}, diurnal meridional currents are of order 0.005 m s^{-1}. We therefore suggest that horizontal advection produces negligible contributions to systematic diurnal variations in salinity.

To summarize, Figure 2 suggests that precipitation, evaporation, and entrainment all likely drive diurnal salinity variations at 156E,2N, with precipitation and entrainment appearing to dominate. The impacts of precipitation and evaporation are highly dependent on the thickness of the layer that they are assumed to vary over (h_P and h_E in equation (2)). Moreover, if h_P and h_E are initially thinner than 1 m, the salinity anomalies driven by precipitation and evaporation will not be detected at the mooring instruments until they are mixed downward; we hypothesize that this can explain the phasing of the local salinity cycle at this mooring, i.e., the lags between precipitation or evaporation and the resulting salinity anomalies. We next extend the observations of diurnal salinity to all mooring sites in order to assess how the forcing regimes at each site contribute to the local salinity variations.

4.2. Spatial Patterns of Daily Surface Salinity Variability

Figure 3a shows the amplitude of the average daily 1 m salinity anomaly at each mooring site. Diurnal salinity amplitudes are small (maximum 0.01 psu and more commonly <0.005 psu), but statistically significant throughout the tropics. Though spatial patterns are irregular, some structure is apparent: amplitudes are largest in the eastern and western tropical Pacific, and along the equator in the Atlantic. In the open ocean (e.g. central Pacific and off-equatorial Atlantic), amplitudes are generally small (<0.002 psu).

The phasing of the daily salinity cycle shows substantial variability across different locations, though in general salinity is minimum between 09:00 and 18:00 (Figure 3b) and maximum between 00:00 and 09:00 (Figure 3c): at 20 of the 35 moorings analyzed, the diurnal salinity cycle had this phasing. The salinity patterns at these sites are generally similar to the example shown in Figure 2, with 1 m salinity increasing as the mixed layer deepens during the night and freshening as the mixed layer shoals in the morning. Slight shifts in the phasing between sites appear to result from subtle differences in the strength and phasing of winds, evaporation, and precipitation. This is illustrated by considering the mooring at 147E,2N, also in the western

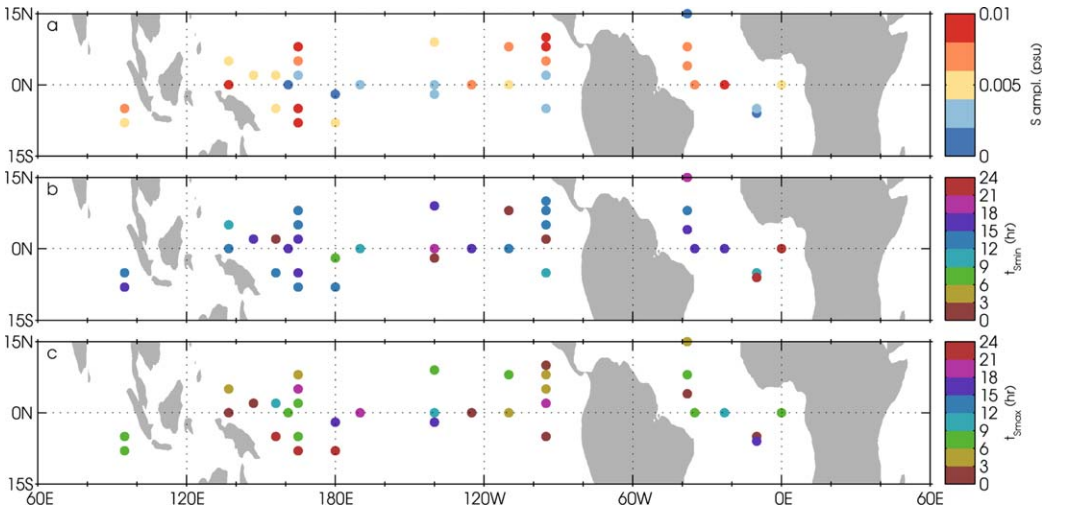

Figure 3. Characteristics of the daily salinity cycle, obtained by fitting diurnal and semidiurnal harmonics to high-passed 1 m depth salinity anomalies at each mooring site: (a) amplitude, computed as half the maximum minus minimum salinities; (b) time of minimum daily salinity (local hour); and (c) time of maximum daily salinity (local hour). Diurnal amplitudes at all sites are statistically significant.

Pacific warm pool (Figure 4). There, early morning precipitation is around twice as strong as at the nearby 156E,2N site (Figure 2b) and appears to drive immediate 1 m freshening beginning at 03:00. However, winds are weak (Figure 4c), which may prevent the surface fresh signal from mixing any deeper into the water column. Indeed, 1 m salinity decreases slowly throughout the day even though precipitation stops by 08:00, and freshening is in fact strongest at around 15:00, which coincides with the onset of afternoon cooling (Figure 4a). This suggests that the freshwater lens produced by morning rainfall remains stable until nighttime convection mixes the surface water downward; salinity at 1 m depth begins increasing at 18:00, once the fresh lens has been mixed away and entrainment brings saltier water upward.

4.3. Drivers of Diurnal Salinity

We have described how the phasing of diurnal salinity anomalies at 156E,2N can result from nighttime entrainment combined with surface-trapped rain and evaporation anomalies that are eventually mixed

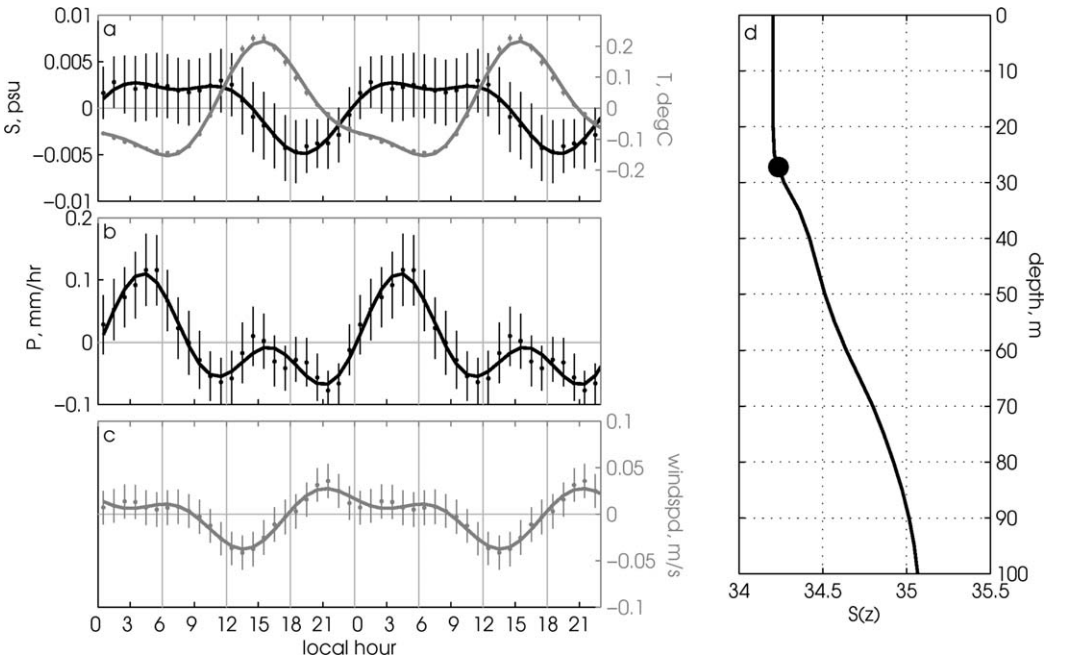

Figure 4. As in Figure 2, but for the mooring at 147E,2N. Evaporation and MLD were not available at this site, so they are not shown.

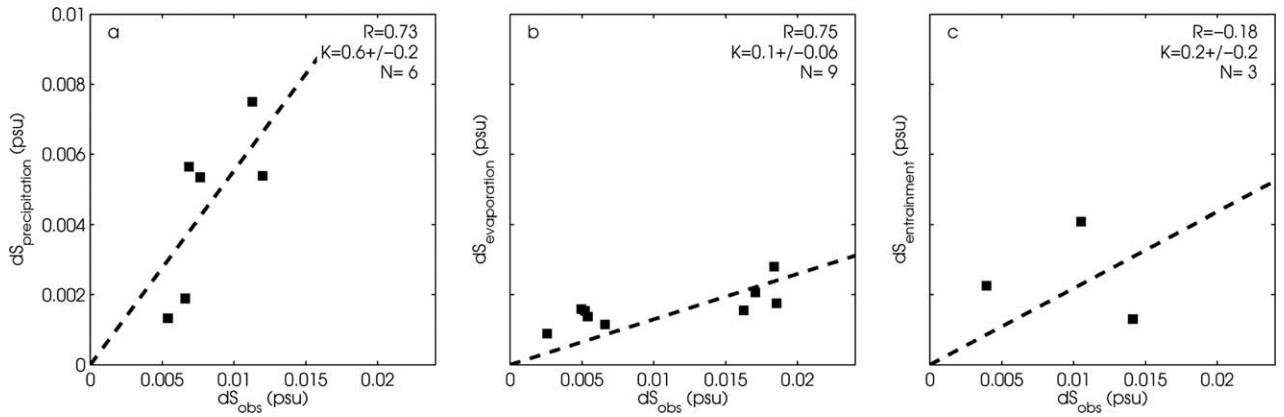

Figure 5. Scatterplots comparing the maximum diurnal salinity anomaly at individual mooring sites (dS_{obs}) to the contribution to diurnal salinity from: (a) precipitation; (b) evaporation; and (c) entrainment. The contribution of each term was estimated using equation (2), with S_o, h, and δS set to their climatological values based on the MIMOC data set, h_P=3 m, and h_E=1 m. Only the mooring sites with sufficient data to estimate the individual terms are shown in each plot; there were no sites with estimates of diurnal precipitation, evaporation, and entrainment, i.e., no site is represented in all three plots. Correlation coefficients (R) are significant at the 95% level for the salinity anomalies related to precipitation and evaporation, but because the entrainment anomaly is based on three data points the correlation is not statistically significant. *K* represents the robust least-squares linear regression, indicating roughly how much each process contributes to diurnal salinity anomalies, on average.

downward by wind -mixing or convective overturning. Phasing of diurnal salinity at the rest of the mooring sites can also be explained using similar arguments (not shown). We next address the question of whether the amplitude of the anomalies at all sites can be explained using observed anomalies of the forcing terms. At the sites for which diurnal cycles of precipitation, evaporation, or mixed-layer depth can be computed, we estimate their associated contributions to the total observed salinity anomaly using equation (2), setting h_P to 3 m and h_E to 1 m and using the local climatological salinity, MLD and salinity jump at the base of the mixed layer. Figure 5 shows that salinity anomalies related to rainfall and evaporation are significantly correlated with the observed diurnal salinity anomaly; the statistics for entrainment are based only on three data points and so are not robust. As noted earlier, diurnal zonal and meridional advection, calculated at four sites, are two orders of magnitude smaller than the observed salinity signal and hence are not shown. The average contribution of each process is estimated by regressing the anomaly produced by that process to the observed diurnal salinity anomaly: this suggests that precipitation produces around 60% of the daily salinity anomaly, entrainment around 20% (noting again that this is based on three data points only), and evaporation around 10%. These regressions are highly dependent on the value of h_P and h_E that were chosen: varying h_P between 1 and 5 m puts the contribution of precipitation at 200% to 30% of the observed salinity; varying h_E from 1 to 3 m puts the evaporation contribution between 10% and 4%. We conclude that diurnal precipitation appears more important for driving diurnal salinity variations than diurnal evaporation. The effect of entrainment cannot be reliably estimated, though these results suggest that its contribution is potentially important.

Based on Figure 5, we can make an educated guess about where diurnal salinity anomalies might be large. Diurnal precipitation and evaporation amplitudes are estimated from the TRMM and HOAPSv3 data sets, respectively (Figure 6a and 6b). Diurnal precipitation is strong throughout the Indo-Pacific warm pool, in the northern Bay of Bengal, in the Gulf of Mexico, and in the far eastern equatorial Pacific and Atlantic Oceans. Diurnal evaporation is strong in somewhat different regions: near coastlines and away from the equator, particularly in the Northern Hemisphere. Diurnal entrainment is more difficult to estimate because it is driven by diurnal variations in MLD, which would require subsurface observations with high temporal and spatial resolution to measure. Such a data set does not exist; however, *Schneider and Müller* [1990], showed that the diurnal amplitude of MLD is significantly correlated with the mean Monin-Obukhov amplitude scale ($\langle \delta L \rangle$), which can be approximated from mean atmospheric conditions. Using the assumption that solar heat flux and winds drive diurnal variations in mixing, and ignoring synoptic-scale variations, *Schneider and Müller* [1990] estimated $\langle \delta L \rangle$ from atmospheric observations of net heat flux (Q_{net}), shortwave radiation (Q_{sw}), and wind stress (τ). Denoting daily mean values with an overbar and long-term averages with $\langle\rangle$, the mean Monin-Obukhov length scale is given by

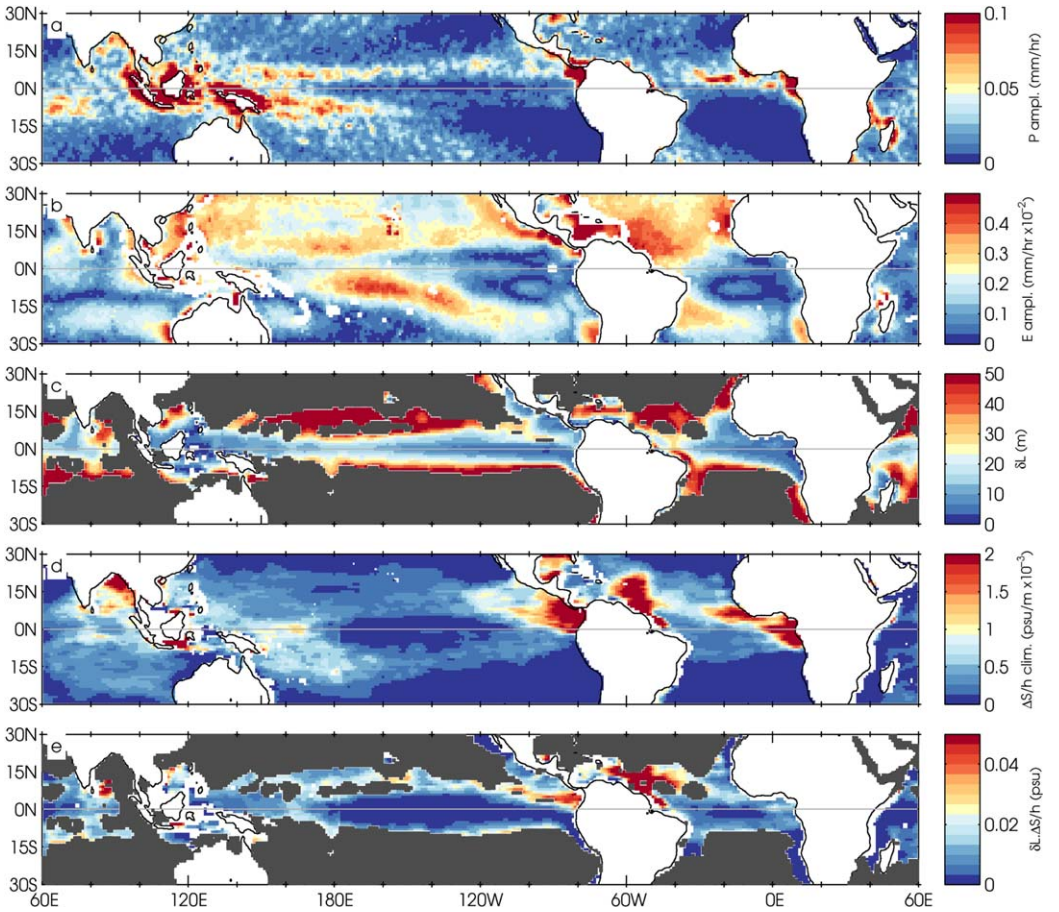

Figure 6. Diurnal amplitude of (a) precipitation, based on TRMM data; and (b) evaporation, based on HOAPSv3.2 data. Note the different color scales for precipitation and evaporation. (c) The mean Monin-Obukhov length scale, a proxy for diurnal MLD (note that the color scale refers to $\langle \delta L \rangle$, not diurnal MLD); regions where net heat flux is smaller than 37 W m^{-2} have been masked out. (d) Salinity jump at the base of the mixed layer scaled by MLD, based on the MIMOC climatology. (e) Entrainment strength, computed as the product of Figures 6c and 6d.

$$\langle \delta L \rangle = \langle \bar{L} \rangle \left[1 - \left(1 + \frac{2\langle \bar{Q}_{sw} \rangle}{\langle \bar{Q} \rangle} \right)^{-1} \right], \tag{3}$$

where $\langle \bar{L} \rangle$, the averaged Monin-Obukhov depth, is given by

$$\langle \bar{L} \rangle = 2 \left(\frac{\langle \tau \rangle}{\rho_o} \right)^{3/2} \left(\frac{\alpha g}{\rho_o c_p} \langle \bar{Q} \rangle \right)^{-1}, \tag{4}$$

where ρ_o is a reference density, α the thermal expansion coefficient, g the gravitational acceleration, and c_p the specific heat. *Schneider and Müller* [1990] used in situ observations to show a linear relationship between $\langle \delta L \rangle$ and the amplitude of diurnal MLD (in regions where net heat flux exceeds 37 W m^{-2}). Using time-averaged heat flux and wind stress data from TropFlux, we estimate $\langle \delta L \rangle$ from equations (3) and (4) (only considering regions for which $\langle \bar{Q} \rangle > 37$ W m^{-2}). This exercise, while not precise, provides insight into regional patterns in the strength of diurnal MLD fluctuations (Figure 6c): for example $\langle \delta L \rangle$ is relatively weak in a band along the equator. To assess where diurnal salinity entrainment is likely to be strong, we multiply $\langle \delta L \rangle$ by climatological $\Delta S/h$, which is essentially a measure of the salinity stratification strength. We emphasize that this product is not an absolute estimate of diurnal salinity entrainment, but instead a rough indication of where it might be strong. Regions where $\Delta S/h$ is large (Figure 6d) indicate a thin mixed layer with a strong salinity jump at its base; if diurnal MLD anomalies are strong, diurnal salinity entrainment will arise. It is unsurprising that Figures 6a and 6d have similar spatial patterns: shallow, salinity-stratified mixed layers are often caused by strong mean precipitation [*de Boyer Montégut et al.*, 2007], and regions with strong

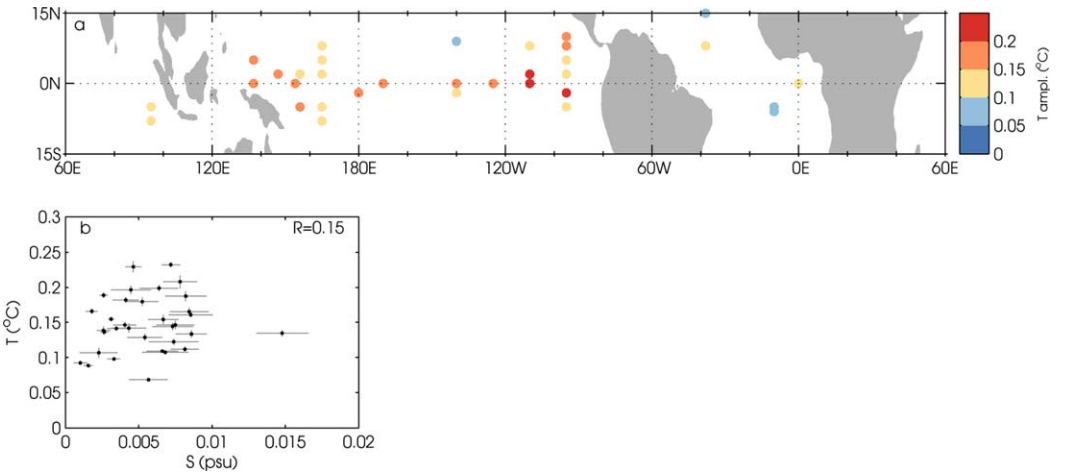

Figure 7. (a) As for Figure 3a, but showing the amplitude of the daily 1 m temperature signal at the 33 mooring sites where enough hourly were available to estimate the diurnal signal. (b) Diurnal amplitude of 1 m temperature plotted against diurnal amplitude of 1 m salinity.

mean precipitation correspond to those with strong diurnal precipitation [*Kikuchi and Wang*, 2008]. Figure 6e indicates that diurnal entrainment is most likely to produce salinity anomalies in the southwestern Bay of Bengal, the Intertropical Convergence Zone of the eastern Pacific Ocean, and the Amazon plume region. In the western Pacific, central Indian, and eastern and western Atlantic Oceans around equator, Figure 6c suggests that diurnal MLD variations are weak but the stratification is so strong that diurnal salinity entrainment may still be significant (Figure 6e). In the central equatorial Pacific Ocean, the entrainment strength is notably weak.

For many of the regions where diurnal precipitation is strongest (Figure 6a), $\langle \delta L \rangle$ cannot be computed so it is difficult to assess the strength of diurnal entrainment. Assuming that diurnal MLD variations are nonnegligible in the masked regions, and considering precipitation and entrainment to be the dominant drivers, we hypothesize that diurnal salinity variability is strong in the Bay of Bengal, around the Indonesian Seas, in the eastern equatorial Atlantic within $\pm 5^\circ$ of the equator, and in the Pacific Intertropical Convergence Zone.

4.4. Diurnal Temperature

Figure 7a shows the amplitude of the diurnal 1 m temperature signal at each of the TAO mooring sites having at least 1 year of hourly temperature data, computed using the same procedure that was used to estimate the diurnal salinity signal. Typical diurnal temperature amplitudes are between 0.1 and 0.2°C, with larger values seen closer to the equator, consistent with being driven by solar insolation. Diurnal temperature peaks at ~15:00 and is minimum at ~06:00 at all sites (not shown), as has been shown previously using observations from Argo profiling floats [Gille, 2012]. Considerable scatter is seen between the amplitudes of diurnal salinity and temperature, and they are not significantly correlated (R=0.15; Figure 7b). This weak correlation suggests that it would be difficult to use diurnal temperature as a proxy for diurnal salinity.

5. Implications of Daily Salinity Variations

5.1. Impacts on Stratification

Diurnal variations in stratification have been shown to affect SST, and hence to be important for air-sea interactions in the tropics [e.g. *Shinoda*, 2005; *Kawai and Wada*, 2007; *Woolnough et al.*, 2007], so it is useful to consider whether daily salinity variations have an appreciable effect on MLD. For the three sites with sufficient subsurface hourly temperature and salinity data to compute the diurnal MLD cycle, we estimate density and MLD in two ways: (1) using hourly salinity, and (2) using daily-averaged salinity. In both cases, we use hourly temperatures and compute density and MLD (as defined in section 3), and estimate the diurnal signals of MLD. At two of the three sites, the daily MLD signal is the same whether computed using hourly or daily salinities (Figure 8b and 8c). At 154E,0N in the far western Pacific Ocean, however, the diurnal amplitude of MLD computed with the hourly salinity is more than 1.5 times as large as that computed with daily salinity. Evidently, the anomalously fresh afternoon conditions (Figure 3b) produce a thinner afternoon mixed layer (Figure 8a). Similarly, the salty morning mixed layer at this site (Figure 3c) produces a much deeper mixed

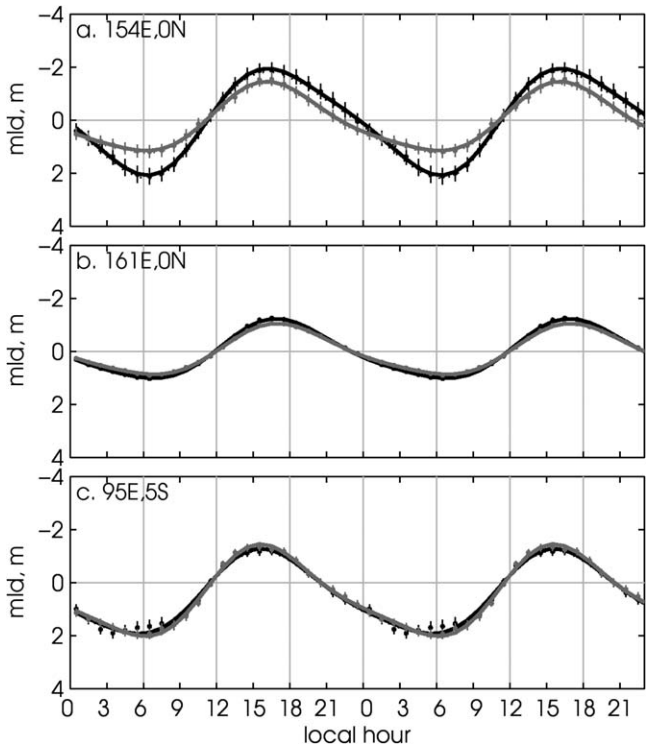

Figure 8. Daily cycles of MLD estimated from density based on hourly temperature and hourly (black) and daily (gray) salinity, at three mooring sites. The markers and lines are as in Figure 2.

layer compared to the daily-average salinity case. The effect of salinity on MLD is asymmetrical throughout the day: morning salinity variations produce a mixed layer around 1 m thicker compared to the daily-mean salinity case, whereas afternoon salinity variations cause only a 0.5 m MLD difference. Potential implications of this finding are described in the discussion section below. Interestingly, at the nearby 161E,0N site, diurnal salinity appears to have no impact on diurnal MLD (Figure 8b) despite being only 7° longitude from the 154E site (Figure 8a).

5.2. Diurnal Salinity and Aquarius

Recall that at a given location, Aquarius samples at the same two times of day: descending nodes in the morning (crossing the equator at around 06:00 local time) and ascending nodes in the evening (18:00 equator crossing). Comparing the ascending-descending salinity difference with the legitimate salinity difference at each mooring site will help in the effort to unravel the uncertainties in salinity measurements from the Aquarius satellite. At each mooring site, we identify the time of the nearest ascending and descending Aquarius overpass and extract the diurnal salinity signal at those two times of day from the mooring data (Figure 3). Then, the "true" salinity anomaly (at each site) that corresponds to the time difference between local ascending and descending Aquarius nodes can be estimated; we refer to this as the "synthetic" δS. Since the ascending Aquarius node is made in the evening, and the descending node in the morning, Figure 9a represents a morning-minus-evening difference, which is generally positive since the daily salinity maximum usually occurs in the morning (Figure 3c). Typical salinity differences between the times of the descending and ascending nodes are on the order of 0.005 psu, with the largest values seen in the western and eastern Pacific Oceans. In the central tropical Pacific Ocean, where the mooring data show maximum salinity in the evening (Figure 3c), salinities at the time of descending Aquarius nodes are smaller than those at the time of ascending passes, i.e., $\delta S_{synthetic}$ is negative (Figure 9a).

If Aquarius salinity estimates had no errors, and the surface layer of the ocean was well-enough mixed that salinity at the 1 m mooring equalled salinity at the true sea surface, differencing the descending-node and ascending-node Aquarius data would give the values shown in Figure 9a. In reality, Aquarius is designed to measure salinities with an accuracy of 0.1 to 0.2 psu on timescales of a week to a month [*Le Vine et al.*, 2007], and individual observations are not expected to resolve 0.005 psu signals. There are uncorrected biases (δS_{bias}) between ascending and descending nodes (see section 3.2) that bury the ascending-descending salinity anomalies that result from legitimate day-night differences (i.e., $\delta S_{synthetic}$). To estimate the magnitude of the ascending-descending bias, we identified the Aquarius measurements made within 100 km of each mooring site, separating data from the ascending and descending Aquarius nodes. At each site, we estimated δS_{bias}, the average difference between the ascending and descending Aquarius salinities. At all sites, the ascending-descending Aquarius bias (Figure 9b) is an order of magnitude greater than the day-night salinity difference derived from the mooring data (Figure 9a). (Note that there is no correlation between the magnitude or sign of δS_{bias} and $\delta S_{synthetic}$). This confirms that with the current Aquarius data

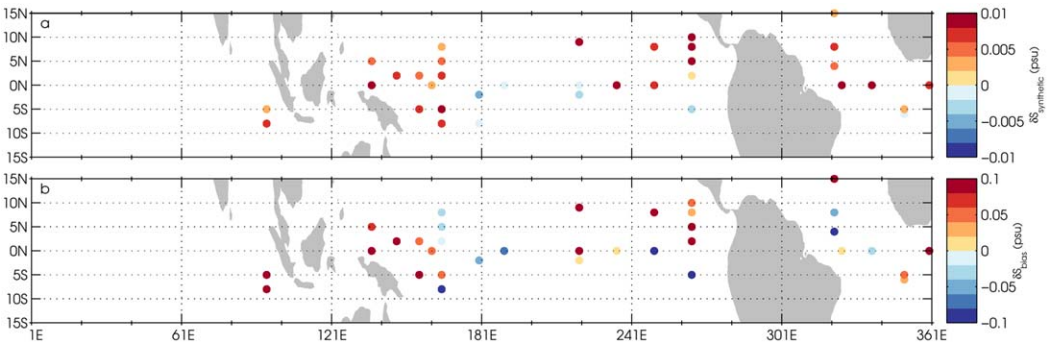

Figure 9. (a) Salinity at the time of the local ascending Aquarius pass (around 18:00) minus salinity at the time of the local descending Aquarius pass (around 06:00). Salinities are taken from the fits to 1 m mooring salinities (Figure 3); only sites with statistically significant fits are plotted. (b) Mean difference between Aquarius descending-node and ascending-node salinities based on Aquarius measurements made within 100 km of each mooring site. Note the different color scales in Figures 9a and 9b.

products, simply differencing the ascending and descending Aquarius nodes is not a viable method for extracting day-night salinity differences.

6. Conclusions and Discussion

Hourly observations from 35 moorings have been used to estimate the average daily variability of 1 m salinity in the tropics. Consistent with three previous studies [*Cronin and McPhaden*, 1999; *Reverdin et al*., 2012] (J. E. Anderson and S. C. Riser, submitted manuscript, 2014), we show that the amplitude of the daily salinity cycle just below the sea surface is small: less than 0.01 psu and more typically around 0.005 psu. A close examination of dynamics at different sites suggests that entrainment and precipitation appear to drive the diurnal salinity cycle (Figure 5). Although we could only estimate the amplitude of entrainment at three locations, it contributed significantly to diurnal salinity anomalies there. We hypothesize that entrainment, which results from nighttime convective overturning as the sea surface cools, drives the daily increase of salinity (with a small contribution from evaporation) and generally sets the phasing of the signal: increasing salinity at night with a peak between 00:00 and 09:00 (Figure 3c). Precipitation drives the subsequent freshening; since rainfall can be trapped in thin lenses, the fresh anomalies may not be detected at 1 m depth until winds or overturning mixes them below the surface. Horizontal salinity advection, estimated at several equatorial sites having near-surface velocity data, was found to have a negligible contribution to diurnal salinity.

While our findings are too speculative to predict the amplitude of diurnal salinity variations, we suggest that the largest salinity anomalies will be found in regions with large diurnal precipitation and mixed-layer depth variations and strong salinity stratification. Based on estimates of diurnal precipitation from the TRMM satellite and $\Delta S/h$ from the MIMOC climatology (Figure 6), these regions include the northern Bay of Bengal, the Indonesian Seas, and the eastern equatorial upwelling regions in the Pacific and Atlantic Oceans. Diurnal entrainment is challenging to estimate because it requires knowledge of diurnal MLD variability. As a proxy, we computed mean Monin-Obukhov length scales following *Schneider and Müller* [1990]. Although it gave some insight into patterns of diurnal entrainment, the method is limited to regions having a net heat flux <37 W m^{-2}, which eliminated most areas outside of the equatorial band. Moreover, it is very much an approximation, and in situ observations and/or modeling studies are needed in order to more accurately quantify diurnal MLD variations throughout the ocean. Argo has previously been used to estimate diurnal variations in subsurface temperature [*Gille*, 2012] and may prove to be a useful tool for quantifying diurnal MLD, particularly with the proliferation of floats having high vertical resolution, which more accurately resolve subtle variations in MLD.

Quantifying the impacts of precipitation and evaporation on diurnal salinity (Figure 5) relied on the assumptions that (a) rain-driven anomalies penetrate to 3 m, an estimate based on the size of a freshwater lens estimated to arise from observed rain events; and (b) evaporation produces surface salinity anomalies that mix down to 1 m depth, which was based on stability analysis of a water parcel undergoing typical rates of evaporation. In fact, rainfall has been shown to drive surface freshening over depths ranging from

centimeters to more than 10 m [*Katsaros and Buettner*, 1969; *Price*, 1979; *Wijesekera et al*., 1999; *Soloviev and Lukas*, 2006; *McCulloch et al*., 2012; *Reverdin et al*., 2012], and the effects of evaporation near the sea surface are not well understood [*Yu*, 2010; *Asher et al*., 2014a]. Precipitation-related and evaporation-related salinity anomalies are highly dependent on local winds and background stratification [*Asher et al*., 2014b] and may change from one day to the next, suggesting that fixed values of h_P and h_E in equation (2) may be an oversimplification. Understanding the three-dimensional dispersion of salinity anomalies on timescales of minutes to days is necessary in order to understand the diurnal cycle of surface salinity, and will require both modeling and observational efforts.

This study has uncertain conclusions regarding the impacts of diurnal salinity variations on upper ocean stratification. It is an important question, as diurnal variations in MLD appear to modulate SST on intraseasonal time scales [*Shinoda*, 2005]. We have shown that at 154E,0N in the western Pacific warm pool, salinity is responsible for half of the average daily variation in MLD, which hints at a potentially substantial role of salinity in air-sea feedback processes. However, less than 1000 km away at 161E,0N, salinity does not appear to affect diurnal MLD. These results are compelling enough to warrant further investigation of the diurnal salinity signal in the tropics.

Finally, we consider diurnal salinity variability in the context of the Aquarius satellite salinity mission. Aquarius is in a sun-synchronous orbit, so that ascending and descending nodes cross a given latitude in the evening and the morning, respectively. For other satellite data sets, this feature has been exploited to extract information about day-night differences—for example, in winds [*Gille et al*., 2003] and SST [*Stuart-Menteth et al*., 2003]. We found that ascending-descending biases in Aquarius data are an order of magnitude greater than the actual day-night salinity anomalies observed at the moorings, indicating that great care must be taken in interpreting day-night differences observed in Aquarius salinities. Our results also have implications if empirical corrections are applied to the ascending-descending biases in Aquarius salinities: actual day-night salinity anomalies are nonzero at the mooring sites, and likely to be large throughout many regions of the tropics (Figure 6). The present study used mooring data at 1 m depth, in contrast to the true SSS that Aquarius measures. A recent study using Argo floats that profile to within 0.2 m of the surface (J. E. Anderson and S. C. Riser, submitted manuscript, 2014) showed that the diurnal salinity signal at that depth can be about an order of magnitude greater than the diurnal salinity signal at 1 m depth, suggesting that diurnal salinity at the sea surface may in fact be strong enough to be comparable to Aquarius ascending-descending SSS differences. This implies that care must be taken in correcting the ascending-descending differences in Aquarius, as some of the apparent bias could potentially contain a legitimate diurnal signal. Fully resolving the relationship between true surface salinity and near surface (e.g. 1 m depth) will require in situ observations of true SSS over numerous diurnal cycles in a variety of locations. Extending current observation networks such as the surface drifter program and Argo floats that profile close to the sea surface will be extremely valuable for this task.

Acknowledgments
We gratefully acknowledge the sources of data for this study: the TAO Project Office of NOAA/PMEL (mooring data) and NOAA (MIMOC climatology), NASA (Aquarius and TRMM data), the World Data Center for Climate (HOAPSv3.2 data), the Indian National Centre for Ocean Information Services (TropFlux data). This work was supported by NASA award NNX13AO38G (J.S., K.D.) and NOAA grant NA10OAR4310139 (S.T.G., K.D.). We thank two anonymous reviewers for their suggestions.

References

Anderson, S., R. Weller, and R. Lukas (1996), Surface buoyancy forcing and the mixed layer of the western Pacific warm pool: Observations and 1D model results, *J. Clim.*, *9*(12), 3056–3085.

Asher, W. E., A. T. Jessup, and D. Clark (2014a), Stable near-surface ocean salinity stratifications due to evaporation observed during STRASSE, *J. Geophys. Res. Oceans*, *119*, 3219–3233, doi:10.1002/2014JC009808.

Asher, W. E., A. T. Jessup, R. Branch, and D. Clark (2014b), Observations of rain-induced near surface salinity anomalies, *J. Geophys. Res. Oceans*, doi:10.1002/2014JC009954.

Bernie, D., S. Woolnough, J. Slingo, and E. Guilyardi (2005), Modeling diurnal and intraseasonal variability of the ocean mixed layer, *J. Clim.*, *18*(8), 1190–1202.

Bernie, D., E. Guilyardi, G. Madec, J. Slingo, and S. Woolnough (2007), Impact of resolving the diurnal cycle in an ocean-atmosphere GCM. Part 1: A diurnally forced OGCM, *Clim. Dyn.*, *29*(6), 575–590, doi:10.1007/s00382-007-0249-6.

Brainerd, K., and M. Gregg (1997), Turbulence and stratification on the tropical ocean-global atmosphere-coupled ocean-atmosphere response experiment microstructure pilot cruise, *J. Geophys. Res.*, *102*(C5), 10,437–10.

Clayson, C. A., and A. S. Bogdanoff (2013), The effect of diurnal sea surface temperature warming on climatological air-sea fluxes, *J. Clim.*, *26*(8), 2546–2556.

Cronin, M. F., and W. S. Kessler (2009), Near-surface shear flow in the tropical Pacific cold tongue front, *J. Phys. Oceanogr.*, *39*(5), 1200–1215.

Cronin, M. F., and M. J. McPhaden (1999), Diurnal cycle of rainfall and surface salinity in the western Pacific warm pool, *Geophys. Res. Lett.*, *26*(23), 3465–3468.

Cronin, M. F., C. W. Fairall, and M. J. McPhaden (2006), An assessment of buoy-derived and numerical weather prediction surface heat fluxes in the tropical Pacific, *J. Geophys. Res. Oceans*, *111*, C06038, doi:10.1029/2005JC003324.

Danabasoglu, G., W. G. Large, J. J. Tribbia, P. R. Gent, B. P. Briegleb, and J. C. McWilliams (2006), Diurnal coupling in the tropical oceans of CCSM3, *J. Clim.*, *19*(11), 2347–2365.

de Boyer Montégut, C., J. Mignot, A. Lazar, and S. Cravatte (2007), Control of salinity on the mixed layer depth in the world ocean: 1. General description, *J. Geophys. Res*, *112*, C06011, doi:10.1029/2006JC003953.
Durack, P. J., and S. E. Wijffels (2010), Fifty-year trends in global ocean salinities and their relationship to broad-scale warming, *J. Clim.*, *23*(16), 4342–4362.
Fairall, C., E. F. Bradley, J. Hare, A. Grachev, and J. Edson (2003), Bulk parameterization of air-sea fluxes: Updates and verification for the COARE algorithm, *J. Clim.*, *16*(4), 571–591.
Fairall, C. W., E. F. Bradley, D. P. Rogers, J. B. Edson, and G. S. Young (1996), Bulk parameterization of air-sea fluxes for tropical ocean-global atmosphere coupled-ocean atmosphere response experiment, *J. Geophys. Res.*, *101*(C2), 3747–3764.
Fennig, K., A. Andersson, S. Bakan, C.-P. Klepp, and M. Schröder (2012), *Hamburg Ocean Atmosphere Parameters and Fluxes from Satellite Data—HOAPS 3.2—Monthly Means/6-Hourly Composites*, [electronic], Satell. Appl. Fac. on Clim. Monit., doi:10.5676/EUM_SAF_CM/HOAPS/V001.
Gille, S. (2012), Diurnal variability of upper ocean temperatures from microwave satellite measurements and Argo profiles, *J. Geophys. Res.*, *117*, C11027, doi:10.1029/2012JC007883.
Gille, S. T., S. G. L. Smith, and S. M. Lee (2003), Measuring the sea breeze from QuikSCAT scatterometry, *Geophys. Res. Lett.*, *30*(3), 1114, doi:10.1029/2002GL016230.
Gille, S. T., S. G. L. Smith, and N. M. Statom (2005), Global observations of the land breeze, *Geophys. Res. Lett.*, *32*, L05605, doi:10.1029/2004GL022139.
Henocq, C., J. Boutin, G. Reverdin, F. Petitcolin, S. Arnault, and P. Lattes (2010), Vertical variability of near-surface salinity in the tropics: Consequences for l-band radiometer calibration and validation, *J. Atmos. Oceanic Technol.*, *27*(1), 192–209.
Huffman, G. J., D. T. Bolvin, E. J. Nelkin, D. B. Wolff, R. F. Adler, G. Gu, Y. Hong, K. P. Bowman, and E. F. Stocker (2007), The TRMM Multisatellite Precipitation Analysis (TMPA): Quasi-global, multiyear, combined-sensor precipitation estimates at fine scales, *J. Hydrometeorol.*, *8*(1), 38–55.
Janowiak, J. E., P. A. Arkin, and M. Morrissey (1994), An examination of the diurnal cycle in oceanic tropical rainfall using satellite and in situ data, *Mon. Weather Rev.*, *122*(10), 2296–2311.
Katsaros, K., and K. J. Buettner (1969), Influence of rainfall on temperature and salinity of the ocean surface, *J. Appl. Meteorol.*, *8*(1), 15–18.
Kawai, Y., and A. Wada (2007), Diurnal sea surface temperature variation and its impact on the atmosphere and ocean: A review, *J. Oceanogr.*, *63*(5), 721–744.
Kikuchi, K., and B. Wang (2008), Diurnal precipitation regimes in the global tropics, *J. Clim.*, *21*(11), 2680–2696.
Kumar, P., J. Vialard, M. Lengaigne, V. Murty, and M. McPhaden (2012), Tropflux: Air-sea fluxes for the global tropical oceans-description and evaluation, *Clim. Dyn.*, *38*, 1521–1543.
Lagerloef, G., F. Colomb, D. Le Vine, F. Wentz, S. Yueh, C. Ruf, J. Lilly, J. Gunn, and Y. Chao (2008), The Aquarius/SAC-D mission: Designed to meet the salinity remote-sensing challenge, *Oceanography*, *21*(1), 68–81.
Le Vine, D. M., G. S. Lagerloef, F. R. Colomb, S. H. Yueh, and F. A. Pellerano (2007), Aquarius: An instrument to monitor sea surface salinity from space, *IEEE Trans. Geosci. Remote Sens.*, *45*(7), 2040–2050.
Li, Y., W. Han, T. Shinoda, C. Wang, R.-C. Lien, J. N. Moum, and J.-W. Wang (2013), Effects of the diurnal cycle in solar radiation on the tropical Indian Ocean mixed layer variability during wintertime Madden-Julian Oscillations, *J. Geophys. Res. Oceans*, *118*, 4945–4964, doi:10.1002/jgrc.20395.
Lien, R.-C., D. R. Caldwell, M. Gregg, and J. N. Moum (1995), Turbulence variability at the equator in the central Pacific at the beginning of the 1991–1993 El Niño, *J. Geophys. Res.*, *100*(C4), 6881–6898.
Lukas, R., and E. Lindstrom (1991), The mixed layer of the western equatorial Pacific Ocean, *J. Geophys. Res.*, *96*(S01), 3343–3357.
Maes, C., B. Dewitte, J. Sudre, V. Garçon, and D. Varillon (2013), Small-scale features of temperature and salinity surface fields in the Coral Sea, *J. Geophys. Res. Oceans*, *118*, 5426–5438, doi:10.1002/jgrc.20344.
McCreary, J. P., K. E. Kohler, R. R. Hood, S. Smith, J. Kindle, A. S. Fischer, and R. A. Weller (2001), Influences of diurnal and intraseasonal forcing on mixed-layer and biological variability in the central Arabian Sea, *J. Geophys. Res.*, *106*(C4), 7139–7155.
McCulloch, M., P. Spurgeon, and A. Chuprin (2012), Have mid-latitude ocean rain-lenses been seen by the SMOS satellite?, *Ocean Modell.*, *43*, 108–111.
Miller, J. R. (1976), The salinity effect in a mixed layer ocean model, *J. Phys. Oceanogr.*, *6*(1), 29–35.
Nesbitt, S. W., and E. J. Zipser (2003), The diurnal cycle of rainfall and convective intensity according to three years of TRMM measurements, *J. Clim.*, *16*(10), 1456–1475.
Price, J. F. (1979), Observations of a rain-formed mixed layer, *J. Phys. Oceanogr.*, *9*(3), 643–649.
Reverdin, G., S. Morisset, J. Boutin, and N. Martin (2012), Rain-induced variability of near sea-surface T and S from drifter data, *J. Geophys. Res.*, *117*, C02032, doi:10.1029/2011JC007549.
Roemmich, D., and J. Gilson (2009), The 2004–2008 mean and annual cycle of temperature, salinity, and steric height in the global ocean from the Argo program, *Prog. Oceanogr.*, *82*(2), 81–100.
Schmidtko, S., G. C. Johnson, and J. M. Lyman (2013), MIMOC: A global monthly isopycnal upper-ocean climatology with mixed layers, *J. Geophys. Res. Oceans*, *118*, 1658–1672, doi:10.1002/jgrc.20122.
Schneider, N., and P. Müller (1990), The meridional and seasonal structures of the mixed-layer depth and its diurnal amplitude observed during the Hawaii-to-Tahiti Shuttle experiment, *J. Phys. Oceanogr.*, *20*(9), 1395–1404.
Shinoda, T. (2005), Impact of the diurnal cycle of solar radiation on intraseasonal SST variability in the western equatorial Pacific, *J. Clim.*, *18*(14), 2628–2636.
Soloviev, A., and R. Lukas (1997), Observation of large diurnal warming events in the near-surface layer of the western equatorial pacific warm pool, *Deep Sea Res., Part I*, *44*(6), 1055–1076.
Soloviev, A., and R. Lukas (2006), The near-surface layer of the ocean: Structure, dynamics and applications, chap. 4, in *Atmospheric and Oceanographic Sciences Library*, vol. 31, Springer, Dordrecht, Netherlands.
Soloviev, A., and N. Vershinsky (1982), The vertical structure of the thin surface layer of the ocean under conditions of low wind speed, *Deep Sea Res., Part A*, *29*(12), 1437–1449.
Sprintall, J., and M. Tomczak (1992), Evidence of the barrier layer in the surface layer of the tropics, *J. Geophys. Res.*, *97*(C5), 7305–7316.
Stuart-Menteth, A. C., I. S. Robinson, and P. G. Challenor (2003), A global study of diurnal warming using satellite-derived sea surface temperature, *J. Geophys. Res.*, *108*(C5), 3155, doi:10.1029/2002JC001534.
Tomczak, M. (1995), Salinity variability in the surface layer of the tropical western Pacific Ocean, *J. Geophys. Res.*, *100*(C10), 20,499–20,515.
Venkatram, A. (1980), Estimating the Monin-Obukhov length in the stable boundary layer for dispersion calculations, *Boundary Layer Meteorol.*, *19*(4), 481–485.

Vialard, J., et al. (2009), Cirene: Air-sea interactions in the Seychelles-Chagos Thermocline Ridge region, *Bull. Am. Meteorol. Soc.*, *90*(1), 45–61.
Wijesekera, H., C. Paulson, and A. Huyer (1999), The effect of rainfall on the surface layer during a westerly wind burst in the western equatorial pacific, *J. Phys. Oceanogr.*, *29*(4), 612–632.
Wijesekera, H. W., and M. C. Gregg (1996), Surface layer response to weak winds, westerly bursts, and rain squalls in the western Pacific Warm Pool, *J. Geophys. Res.*, *101*(C1), 977–997.
Woods, J. (1980), Diurnal and seasonal variation of convection in the wind-mixed layer of the ocean, *Q. J. R. Meteorol. Soc.*, *106*(449), 379–394.
Woods, J. D., W. Barkmann, and A. Horch (1984), Solar heating of the oceansdiurnal, seasonal and meridional variation, *Q. J. R. Meteorol. Soc.*, *110*(465), 633–656.
Woolnough, S., F. Vitart, and M. Balmaseda (2007), The role of the ocean in the Madden-Julian Oscillation: Implications for MJO prediction, *Q. J. R. Meteorol. Soc.*, *132*(622), 117–128.
Yu, L. (2010), On sea surface salinity skin effect induced by evaporation and implications for remote sensing of ocean salinity, *J. Phys. Oceanogr.*, *40*(1), 85–102, doi:10.1175/2009JPO4168.1.
Yueh, S. (2013), *Aquarius CAP Algorithm and Data User Guide*, 2nd ed., Jet Propul. Lab., Pasadena, Calif.